

Ultrafast Terahertz and Optical Spectroscopy under Synergetic Extreme Conditions

Xinbo Wang,^{1,2,*} Tao Dong,^{3,4} Jianlin Luo,^{1,2} and Nanlin Wang^{3,4}

¹*Beijing National Laboratory for Condensed Matter Physics,*

Institute of Physics, Chinese Academy of Sciences, Beijing 100190, China

²*School of Physical Sciences, University of Chinese Academy of Sciences, Beijing 100190, China*

³*Tsung-Dao Lee Institute, Department of Physics and Astronomy, Shanghai Jiao Tong University*

⁴*International Center for Quantum Materials, School of Physics, Peking University, Beijing 100871, China*

(Dated: June 16, 2026)

Elucidating and manipulating emergent phases in complex materials requires direct access to their low-energy collective modes. Terahertz (THz) time-domain and ultrafast optical spectroscopies have emerged as indispensable experimental tools, enabling the probing of intrinsic electrodynamics and the coherent control of non-equilibrium states. At the Synergetic Extreme Condition User Facility (SECUF), we have developed a suite of intense ultrashort light sources covering the near-infrared, mid-infrared, and THz spectral ranges. By integrating these strong-field pulses with extreme sample environments, such as low temperatures, strong magnetic fields, and high pressures, we have established several state-of-the-art spectroscopy platforms. In this article, we outline the technical specifications of each setup and highlight representative user experiments. The presented results underscore the exceptional capability of the THz experimental unit (A4-2) to explore ultrafast dynamics across a multi-parameter thermodynamic phase space.

1. Introduction

Terahertz (THz) radiation bridges the spectral gap between microwaves and infrared light, typically ranging from 0.1 to 30 THz (1 THz \approx 4.1 meV) within the electromagnetic spectrum. In condensed matter physics, the characteristic energy scales of elementary excitations, such as phonons, magnons, excitons, and superconducting gaps, fall within the THz and mid-infrared (MIR) frequency regimes [1–4]. Terahertz time-domain spectroscopy (THz-TDS) provides a unique phase-resolved experimental tool to directly probe the linear electrodynamic response of these low-energy modes [5]. Over the past decade, the study of light-matter interactions has experienced a profound paradigm shift from weak-field probing to strong-field coherent control [6, 7]. Intense THz and MIR pulses can resonantly pump specific collective excitations, driving quantum materials far from equilibrium to trigger pronounced nonlinear optical effects and exotic transient quantum phase transitions, spanning from light-induced superconductivity [8–10] to ultrafast coherent magnetic switching [11, 12].

While intense light pulses drive quantum materials far from equilibrium, the resulting transient dynamics are dictated by their initial thermodynamic ground states [6, 7]. Applying extreme experimental conditions, such as low temperatures, strong magnetic fields, and high pressures, enables the systematic investigation of complex phase diagrams across diverse quantum materials [13, 14]. For instance, an external magnetic field provides a clean tuning knob to manipulate spin configurations and electronic topologies, whereas hydrostatic pressure continuously modulates the electronic bandwidth and electron-lattice interactions without introducing chemical disorder [15]. Integrating ultrafast optical spectroscopies with such demanding environments constitutes a major frontier in

experimental physics [4]. However, achieving this synergetic integration encounters formidable technical challenges, particularly for intense THz and MIR techniques [16]. The difficulties stem from the inherent complexities in generating intense long-wavelength pulses and efficiently coupling them into the spatially restricted optical accesses of extreme sample environments [17].

In 2018, the initial design for the infrared and THz experimental stations at the Synergetic Extreme Condition User Facility was proposed [18]. Following four years of successful commissioning, this article presents the established spectroscopic capabilities of the operational THz experimental unit (A4-2). We first introduce the THz time-domain spectroscopy coupled with low temperatures and strong magnetic fields. Next, we detail the generation of intense THz and mid-infrared sources and their associated pump-probe platforms, including THz-pump optical-probe techniques, THz third-harmonic generation, and THz two-dimensional coherent spectroscopy. We highlight the key scientific advances achieved by users on these respective platforms. Furthermore, we discuss the optical pump-probe spectroscopy integrated with high-pressure diamond anvil cells. Finally, we conclude this article with a perspective on future opportunities.

2. Ultrafast Terahertz and Optical Spectroscopy Platforms

2.1. Terahertz Time-Domain Spectroscopy

Probing energy gaps and collective modes in complex materials requires precise measurements of the low-energy electrodynamics [1, 5]. To investigate the linear responses under synergetic extreme conditions, we have integrated a fiber-coupled THz spectrometer based on photoconductive antennas with a split-coil superconducting magnet system (Fig. 1a). The platform is equipped with a variable temperature insert to achieve low temperatures down to 1.5 K alongside magnetic fields up to 10 T. The entire magnet assembly is mounted on

* xinbowang@iphy.ac.cn

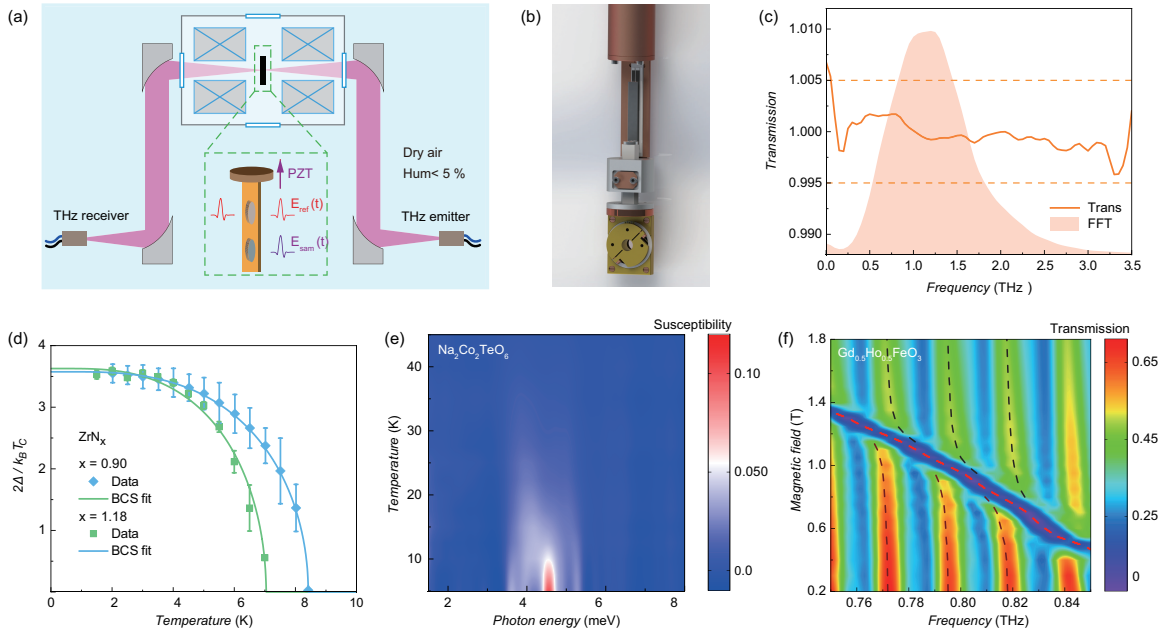


FIG. 1. (a) Schematic illustration of the THz spectrometer coupled with a split-coil superconducting magnet. (b) Detailed view of the PZT-driven linear and rotation stages mounted at the end of the sample rod. In THz-TDS measurements, the rotation stage is replaced by the customized sample holder shown in (a). Adapted with permission from Ref. [17]. Copyright 2024 AIP Publishing. (c) Vacuum-to-vacuum transmittance of two 2.5-mm-diameter apertures. (d) Temperature dependence of the derived superconducting energy gap for the disordered ZrN_x films, with solid lines representing the standard BCS fit. Adapted with permission from Ref. [20]. Copyright 2023 Science China Press. (e) Color map of the imaginary part of the magnetic susceptibility for the Kitaev quantum spin liquid candidate $\text{Na}_2\text{Co}_2\text{TeO}_6$, measured under a 10 T in-plane magnetic field. Adapted with permission from Ref. [21], Copyright 2025 by the American Physical Society. (f) Magnetic field-dependent THz transmittance contour plot of *b*-cut $\text{Gd}_{0.5}\text{Ho}_{0.5}\text{FeO}_3$ single crystal at 2 K. Adapted with permission from Ref. [24]. Copyright 2025 AIP Publishing.

a linear stage and a swing bearing, permitting a 90° rotation of the magnetic field relative to the terahertz propagation direction [17]. The mechanical design guarantees a convenient transition between the Faraday and Voigt configurations without altering the optical alignment. Furthermore, a piezoelectric (PZT)-driven linear stage with a travel range of 20 mm is installed at the end of the sample rod for precise vertical translation (Fig. 1b). It enables automated *in situ* switching between the sample and reference apertures at low temperatures and high magnetic fields, thereby substantially enhancing measurement reliability and data acquisition efficiency.

In THz-TDS measurements, the customized sample holder permits the simultaneous loading of multiple samples and references. The time-domain waveforms of the THz electric fields transmitted through the sample $E_{\text{sam}}(t)$ and the reference $E_{\text{ref}}(t)$ are recorded sequentially under identical experimental conditions. Following Fourier transformation, the complex transmission spectrum $\tilde{T}(\omega) = \tilde{E}_{\text{sam}}(\omega)/\tilde{E}_{\text{ref}}(\omega)$ is obtained [5]. Notably, utilizing empty apertures with a 2.5-mm diameter, the platform demonstrates a near-unity transmission baseline with amplitude fluctuations less than 0.5% across an effective spectral range of 0.1 to 3.5 THz (Fig. 1c). By iteratively solving the Fresnel equations that account for the sample thickness and internal multiple reflections, the complex optical constants are rigorously extracted without resorting to Kramers-Kronig transformations [19].

The obtained optical constants provide unambiguous signatures of charge and spin dynamics. For superconductors, the energy gap can be identified from the suppression in the real part of the optical conductivity below the transition temperature, as recently demonstrated in the disordered superconductor ZrN_x film [20]. The derived superconducting gap follows the standard Bardeen-Cooper-Schrieffer (BCS) temperature dependence (Fig. 1d). This result indicates a conventional electron-phonon coupling mechanism, providing critical insights into the microscopic origin of its anomalous superconducting dome. For collective magnetic excitations, the application of high magnetic fields at low temperatures allows the probing of field-induced spin responses, which manifest as well-defined resonances in the complex magnetic susceptibility. A representative study focuses on the Kitaev quantum spin liquid candidate $\text{Na}_2\text{Co}_2\text{TeO}_6$ [21]. As illustrated in the color map of Fig. 1e, under an in-plane magnetic field of 10 T, a broad fractionalized spin excitation continuum is clearly resolved. Remarkably, the excitation continuum persists up to 40 K, substantiating the survival of strong spin correlations and intense quantum fluctuations deep into the paramagnetic regime. Moreover, this platform facilitates the precise manipulation of intricate exchange interactions in rare-earth orthoferrites. Related studies include the discovery of anomalous splitting, merging, and re-splitting magnon behaviors in $\text{Gd}_{0.3}\text{Ho}_{0.7}\text{FeO}_3$ [22], the magnetic-field control of electromagnons in $\text{Dy}_{0.9}\text{Nd}_{0.1}\text{FeO}_3$ [23], and the realization of strong

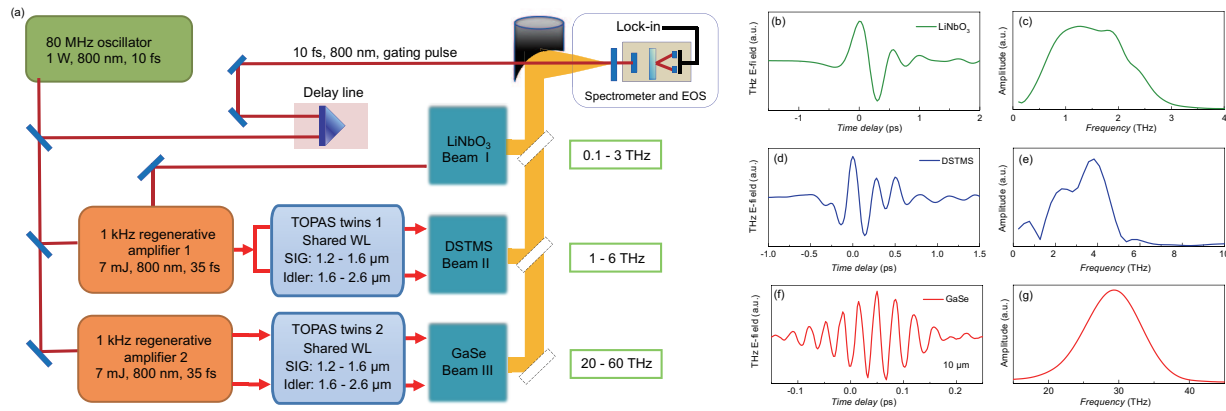


FIG. 2. (a) Schematic layout of the intense laser sources driven by two synchronized high-power Ti:sapphire amplifiers, each coupled with a dual-output optical parametric amplifier, following the initial proposal [18]. The distinct nonlinear frequency conversion pathways and their corresponding spectral coverages are indicated. (b)–(g) Typical time-domain waveforms and corresponding Fourier-transformed spectra for the three high-field sources: (b) and (c) low-frequency THz pulses from optical rectification in LiNbO₃ crystal; (d) and (e) broadband THz pulses from the organic crystal DSTMS; (f) and (g) carrier-envelope-phase-stable MIR transients at a 10- μ m central wavelength generated via difference-frequency-generation in GaSe crystal.

TABLE I. Summary of key experimental parameters for the intense THz and MIR sources. Abbreviations: TPF (tilted-pulse-front), OR (optical rectification), DFG (difference-frequency generation). Symbols used: λ (pump wavelength), E_p (pump pulse energy), \mathcal{E} (THz/MIR output pulse energy), d (focal spot diameter), and E_{THz} (peak electric field). The values represent typical performance parameters characterized under optimal focusing conditions. As a representative MIR example, the intense 12.5 μ m pulse is generated via DFG between two signal beams (1380 nm and 1550 nm), with its corresponding driving and output parameters tabulated.

Source	Freq. (THz)	Generation Scheme	Pump Parameters		Efficiency (%)	THz/MIR Output		
			λ (nm)	E_p (mJ)		\mathcal{E} (μ J)	d (μ m)	E_{THz} (MV/cm)
LiNbO ₃	0.1 – 3	TPF	800	5.5	0.4	20	500	1
DSTMS	1 – 6	OR	1350	0.40	0.1	5	90	Several
GaSe	20 – 60 (e.g., 24 THz / 12.5 μ m)	DFG	1380 1550	0.38 0.30	1.5	10	< 50	Tens

THz cavity magnon-polaritons in Gd_{0.5}Ho_{0.5}FeO₃, where the high-quality crystal itself acts as a Fabry-Pérot cavity [24]. As depicted in the contour plot of Fig. 1f, by dynamically tuning the magnon modes across the cavity resonances via external magnetic fields, anti-crossing dispersions with pronounced vacuum Rabi splitting are observed, confirming the strong light-matter interaction regime [24]. These compelling demonstrations validate the platform’s exceptional capability to uncover the intrinsic ground states and cooperative excitations of quantum materials.

2.2. Ultrafast Terahertz Nonlinear Spectroscopy

2.2.1. High-Intensity Terahertz and Mid-Infrared Sources

To drive quantum materials far from equilibrium and enable the coherent control of their emergent properties, it is imperative to develop high-intensity THz sources [25–27]. The THz experimental unit (A4-2) is equipped with two synchro-

nized Ti:sapphire amplifiers delivering 35-fs, 7-mJ pulses at a 1-kHz repetition rate, each coupled with a dual-output optical parametric amplifiers (OPAs). Through nonlinear frequency conversion, three intense THz sources have been established, as outlined in Fig. 2, spanning a broad spectral range from 0.1 to 60 THz.

First, for the low-frequency regime from 0.1 to 3 THz, vertically polarized THz pulses are generated in a MgO-doped LiNbO₃ crystal, which is pumped by the primary fundamental output of the first amplifier. A reflective diffraction grating is utilized to tilt the pump-pulse front to effectively compensate for the large velocity mismatch between the near-infrared pump and the generated THz wave [28]. The optimized configuration achieves a pump-to-THz energy conversion efficiency of approximately 0.4%, providing a maximum THz pulse energy exceeding 20 μ J [17, 29]. We can tightly focus the THz beam to a $1/e^2$ spot diameter of 0.5 mm, reaching a peak electric field larger than 1 MV/cm with a center frequency of 0.8 THz [30].

Second, to access higher THz frequencies from 1 to 6 THz,

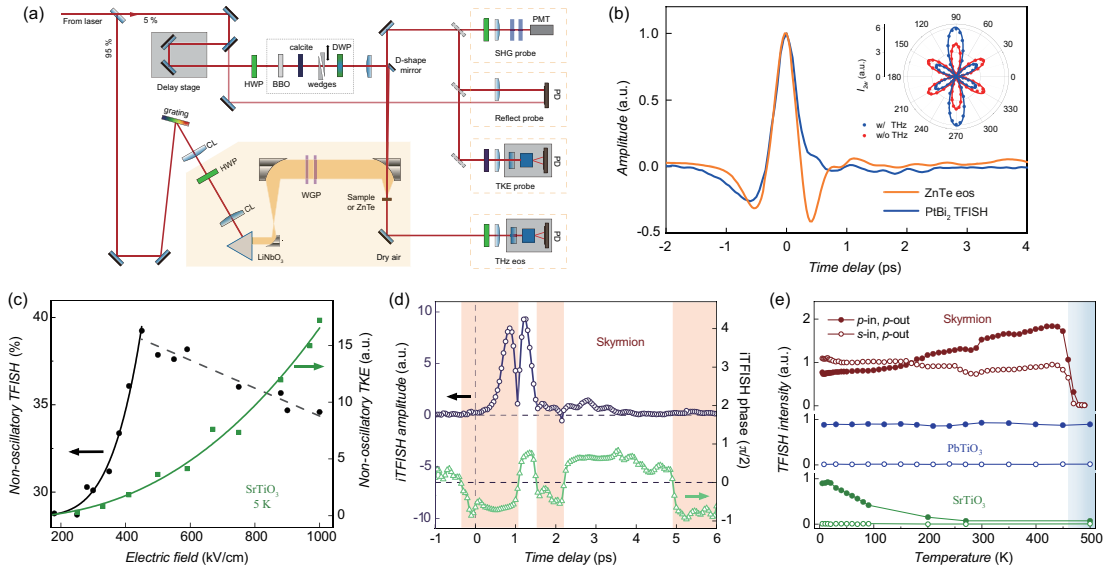


FIG. 3. (a) Schematic diagram of the THz-pump optical-probe setup incorporating an interferometric second-harmonic generation module for phase-sensitive detection. (b) Transient SHG enhancement in the topological semimetal PtBi₂ following the incident THz waveform, with the inset displaying the SHG polar plot under a parallel configuration. Adapted with permission from Ref. [38]. Copyright Optical Society of America. (c) Field-dependent amplitudes of the non-oscillatory TFISH component and the TKE signal in SrTiO₃ at 5 K. Adapted from Ref. [40]. (d) Time-domain iTFISH measurements of polar skyrmions in PbTiO₃/SrTiO₃ superlattices, resolving distinct phase inversions. (e) Temperature dependence of the peak TFISH responses for polar skyrmions, alongside reference measurements on PbTiO₃ thin films and SrTiO₃ single crystals, measured up to 500 K. Panels (d) and (e) are adapted with permission from Ref. [37]. Copyright 2025 Springer Nature.

we employ optical rectification in organic crystals. Specifically, DSTMS possesses a large nonlinear optical coefficient but requires near-infrared driving pulses in the wavelength range of 1300 to 1500 nm to satisfy the phase-matching condition [31]. Driven by the 400- μJ , 1350-nm signal output from one of the optical parametric amplifiers (OPAs, TOPAS twins), the source generates broadband THz pulses with an initial measured energy of 5 μJ . This value is obtained after the generation crystal through three 20-THz low-pass filters, which are necessary to block the residual pump. Since the shorter THz wavelengths enable a tighter focus, the THz beam is focused to a spot diameter of 90 μm . The resulting peak electric field reaches several MV/cm, offering exceptionally high field strengths for broadband nonlinear excitations [32].

Third, for the mid-infrared regime, pulses are generated via difference frequency generation (DFG) in GaSe crystal [33]. By adjusting the wavelengths of the two signal outputs from the TOPAS twins, the resulting MIR radiation can be continuously tuned from 5 to 15 μm (20 to 60 THz). For example, when pumped by the 1380-nm (380 μJ) and 1550-nm (300 μJ) signal beams, the DFG in 1-mm-thick GaSe crystal delivers a typical single-pulse energy of 10 μJ at 12.5 μm . Because these pump beams originate from the twin OPAs sharing the same white-light seed, the MIR transients are passively carrier-envelope-phase stable [34]. The rapidly oscillating MIR electric fields can be resolved in the time domain via electro-optic sampling with sub-20-fs gating pulses. Benefiting from the substantially shorter wavelengths in the MIR regime, the pulses can be tightly focused to a spot size of < 50 μm . Consequently, the peak electric field reaches tens of MV/cm [25]. Coupled with its broad spectral tunability,

this extreme field goes far beyond driving conventional nonlinear lattice dynamics. It provides a versatile tool for mode-selective resonant excitation, pushing specific phonon modes into highly anharmonic regimes and triggering the emergence of novel non-equilibrium states [25].

The dual-amplifier laser system provides intense THz and MIR sources, with their optimal parameters achieved under free-space focusing conditions, as summarized in Table I. The peak electric field of the THz and MIR pulses scales as $E_{\text{THz}} \propto \sqrt{\mathcal{E}}/d$, where \mathcal{E} represents the pulse energy and d denotes the focal spot diameter [35]. Integrating these high-intensity sources with extreme sample environments, such as low temperatures and high magnetic fields, inevitably attenuates the available field at the sample position. The reduction stems primarily from propagation losses through various optical elements and windows along the beam path, combined with the strict geometric constraints of cryostats and magnets that necessitate long-focal-length off-axis parabolic mirrors for focusing [17]. To demonstrate the platform's advanced capabilities for nonlinear optical manipulation, representative probing techniques, including intense THz-pump optical-probe spectroscopy, THz high-harmonic generation, and THz two-dimensional coherent spectroscopy, are detailed in the following subsections.

2.2.2. Terahertz-Pump Optical-Probe Spectroscopy

In a typical pump-probe geometry (Fig. 3a), an intense THz pump and a temporally delayed optical probe are focused collinearly onto the sample at near-normal incidence to trace

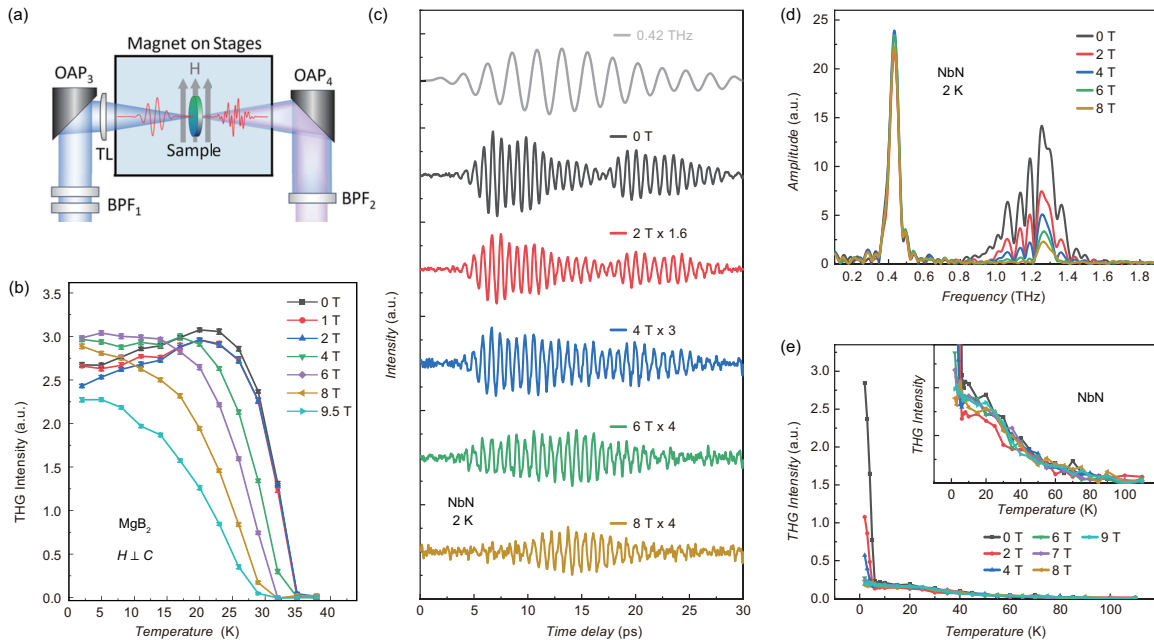


FIG. 4. (a) Detailed diagram of the tight-focusing geometry combining an off-axis parabolic (OAP) mirror and a high-density polyethylene lens (TL). Bandpass filters (BPFs) are used for multi-cycle pumping and THG extraction. (b) Temperature dependence of the THG intensity in MgB₂ under various out-of-plane magnetic fields. Adapted with permission from Ref. [17]. Copyright 2024 AIP Publishing. (c) Time-domain THG waveforms and (d) the corresponding Fourier-transformed spectra for a disordered NbN thin film measured at 2 K under various magnetic fields. (e) Temperature and magnetic-field evolution of the THG intensity in the disordered NbN film, with the inset providing a magnified view of the magnetic-field dependence in the high-temperature normal state. Panels (c)–(e) are adapted with permission from Ref. [44]. Copyright 2026 by the American Physical Society.

the ultrafast nonequilibrium dynamics. We can selectively monitor distinct transient optical responses. Specifically, transient reflectivity ($\Delta R/R$) tracks quasiparticle relaxation, the THz Kerr effect (TKE) measures transient birefringence; and THz-field-induced second harmonic generation (TFISH) probes inversion symmetry breaking. Because conventional TFISH measures only the intensity of the second-harmonic light, the phase information of the emitted field is inherently lost. To overcome this limitation, an interferometric TFISH (iTFISH) module is implemented. A β -barium borate (BBO) crystal generates a 400 nm local oscillator (LO), while a calcite crystal compensates the bulk group velocity dispersion between the 800 nm probe and the 400 nm LO, with a pair of fused silica wedges providing precise phase modulation. The interference between the TFISH from the sample and the LO enables phase sensitive detection, thereby extracting the sign of specific nonlinear tensor elements [36, 37].

Combining intense THz excitations with these optical probes facilitates the direct manipulation and detection of hidden quantum phases. In the topological semimetal PtBi₂, intense THz fields perturb the linear dispersion bands near the Fermi level, producing a 45% enhancement in the transient SHG signal that follows the THz waveform (Fig. 3b) [38]. In the quantum paraelectric SrTiO₃, resonant excitation of the ferroelectric soft mode initiates complex structural dynamics. While previous studies suggested a THz-induced ferroelectric state [39], driving the soft mode into a second-order excited state with elevated THz fields exceeding 500 kV/cm unveils a

reentrant phase transition into a hidden quantum paraelectric phase, as identified by the contrasting field-dependent behaviors of the TFISH and TKE signals (Fig. 3c) [40]. Furthermore, THz-driven coherent control extends to topological polar skyrmions in PbTiO₃/SrTiO₃ superlattices, where the THz pulses couple to the collective modes of the skyrmion walls, giving rise to a hidden phase with a transient macroscopic planar polarization [37]. Crucially, the iTFISH technique successfully resolves distinct phase inversions in the time domain (Fig. 3d), providing direct evidence of the polarization flipping governed by the competition among multiple excited collective modes. The light-induced phase transition is sustained over a broad temperature range up to 470 K (Fig. 3e), due to the intrinsic topological protection of the skyrmion collective modes rather than conventional soft mode dynamics [37]. The precise extraction of these diverse and subtle transient phenomena, ranging from perturbative electronic responses to complex collective mode competitions, demonstrates the capability of the TPOP platform to capture ultrafast quantum dynamics across broad temperature ranges under strong driving fields (~ 1 MV/cm).

2.2.3. Terahertz High-Harmonic Generation Spectroscopy

Nonlinear THz high-harmonic generation spectroscopy requires intense narrowband excitations to resonantly drive non-perturbative electron dynamics and collective excitations [26,

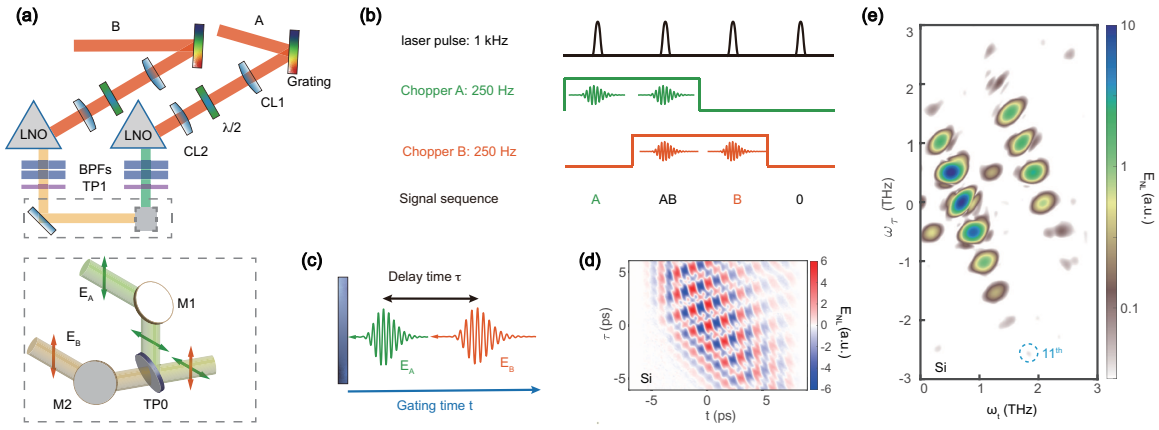


FIG. 5. (a) Experimental design of the 2D-THz coherent spectroscopy platform employing dual LiNbO₃ crystals and a customized periscope-based beam combiner. (b) Pulse sequence and modulation scheme for isolating the pure nonlinear signal in 2D-THz experiments. (c) Timing sequence of the two-pulse excitation defining the time delays. (d) Measured 2D time-domain and (e) corresponding frequency-domain nonlinear responses of n-doped silicon under 0.5-THz and 0.7-THz dual-frequency excitations at room temperature. Adapted with permission from Ref. [29]. Copyright 2024 AIP Publishing.

41]. While intense narrowband THz radiation is predominantly available at free-electron laser facilities which have enabled THz high harmonic-generation in quantum materials [42, 43], tabletop systems can utilize specific band-pass filters to extract the desired frequency components from a broadband source, at the cost of attenuating the electric field strength. Integrating these tailored excitations with low temperatures and high magnetic fields provides an essential means to disentangle competing quantum orders. However, the large physical dimensions of the superconducting magnet cryostat enforce long-focal-length optics, resulting in a large diffraction-limited spot size that further weakens the THz electric field.

To address this challenge, we employ a hybrid focusing geometry comprising an off-axis parabolic mirror and a high-density polyethylene lens to tightly focus the high-energy THz pulses generated from the LiNbO₃ crystal into the magnet center (Fig. 4a) [17]. At the sample position, the peak driving electric field reaches 500 kV/cm for monocycle waveforms and 30 kV/cm for 0.5-THz narrowband excitations. To demonstrate the capabilities of the magneto-THz nonlinear platform, we investigated the THG response of the two-band superconductor MgB₂ [17]. Utilizing the motorized rotation stage (Fig. 1b), *in situ* azimuthal rotation was performed to resolve the polarization dependence of the nonlinear emission without altering the incident THz polarization. Furthermore, applying an out-of-plane magnetic field rapidly suppresses the smaller π -band gap, effectively quenching the THG resonance peak (Fig. 4b). By integrating strong-field THz capabilities with extreme sample environments (up to 10 T and down to 1.5 K), this instrument overcomes the focal distance limitations of conventional table-top systems, providing a robust platform for exploring magnetic-field-dependent nonlinear quantum dynamics.

The capability of this platform to resolve diverse higher-order nonlinear optical phenomena is exemplified by the study of disordered NbN thin films near the superconductor-

insulator transition [44]. Upon excitation with 0.42-THz multicycle pulses, the sample emits a third-harmonic signal that is clearly resolved in both the time and frequency domains (Fig. 4c and 4d). Strikingly, an anomalous THG signal persists above the superconducting transition temperature of approximately 6 K and remains unchanged even when a 9-T magnetic field fully suppresses the global phase coherence (Fig. 4e). Such magnetic-field insensitivity demonstrates that the normal-state nonlinearity originates from disorder-induced band structure modifications rather than superconducting fluctuations. Below the critical temperature, the THG emission from the driven Higgs mode interferes with the coexisting normal-state channel, manifesting as a temporal beating waveform and a broadened multi-peak spectrum [44].

2.2.4. Terahertz Two-Dimensional coherent Spectroscopy

Extending beyond conventional one-dimensional nonlinear techniques, two-dimensional THz (2D-THz) coherent spectroscopy provides a transformative method for probing and controlling multicorrelations in quantum matter [27]. It measures the nonlinear response arising from the interaction between two intense THz pulses as a function of both the interpulse delay and the detection time (Fig. 5b and 5c). Applying a two-dimensional Fourier transform then converts the temporal signals into the frequency domain, which can disentangle multi-order quantum pathways and isolate overlapping collective modes. To realize these demanding measurements, we have developed a versatile 2D-THz platform equipped with dual high-intensity sources generated from separate LiNbO₃ crystals [29]. A customized periscope-based beam combiner merges the high-energy THz beams, ensuring spatiotemporal overlap while preserving their peak electric fields (Fig. 5a). The dual-source design provides the experimental flexibility to independently control the polarization, spectrum, and amplitude of each driving pulse. To demonstrate the instrument's

3. Conclusion and Perspectives

Over the past years, the THz experimental unit (A4-2) at SECUF has successfully transitioned from an initial conceptual design into a comprehensive research platform [18]. By coupling ultrafast optical technologies with extreme sample environments, the facility provides a versatile suite of spectroscopic capabilities, currently primarily utilizing LiNbO₃-based intense THz sources for various pump-probe configurations. The instrumental developments across these setups include achieving peak THz fields of ~ 1 MV/cm in the TPOP system, integrating 10-T magnetic fields down to 1.5 K for magneto-THz-THG measurements, realizing 2D-THz coherent spectroscopy driven by dual independently controlled intense pulses, and incorporating high-pressure and low-temperature environments into the OPOP configuration. As demonstrated by recent experimental studies, these established capabilities provide a rigorous and highly competitive experimental foundation for exploring ultrafast quantum dynamics.

To further expand the spectral coverage, polarization states, and excitation capabilities, continuous efforts are dedicated to developing advanced light sources. First, various nonlinear optical materials, including organic crystals and SiC, are being implemented to generate highly intense transients, effectively bridging the conventional frequency gap between 5 and 15 THz [34, 48]. Furthermore, advanced nonlinear optical techniques, employing chirped-pulse difference frequency generation, are being developed to generate narrowband THz and MIR pulses [49, 50]. Additionally, as existing sources

are predominantly linearly polarized, dedicated efforts are underway to provide intense circularly polarized THz and MIR fields, offering a powerful tool for manipulating chiral and magnetic excitations[51, 52]. Finally, integrating these versatile light sources with extreme sample environments encompassing temperatures down to 1.5 K, magnetic fields up to 10 T, and quasi-hydrostatic pressures up to 35 GPa constitutes a powerful framework for exploring non-equilibrium dynamics.

As a user facility, the THz experimental unit actively seeks broad scientific collaborations. We sincerely invite researchers from the global scientific community to submit experimental proposals and utilize this integrated platform to coherently manipulate complex systems and unravel the underlying physics of emergent phenomena across diverse scientific disciplines.

4. Acknowledgements

This work was supported by the National Key Research and Development Program of China (Grants No. 2024YFA1611300) and the National Natural Science Foundation of China (Grants No. 12574349). We gratefully acknowledge the user community for their collaborative efforts at the THz experimental unit, whose contributions have led to both the representative results discussed in this review and many other ongoing research projects. This work was carried out at the Synergetic Extreme Condition User Facility (SECUF, <https://cstr.cn/31123.02.SECUF>).

-
- [1] D. N. Basov, R. D. Averitt, D. van der Marel, M. Dressel, and K. Haule, Electrodynamics of correlated electron materials, *Rev. Mod. Phys.* **83**, 471 (2011).
 - [2] R. Ulbricht, E. Hendry, J. Shan, T. F. Heinz, and M. Bonn, Carrier dynamics in semiconductors studied with time-resolved terahertz spectroscopy, *Rev. Mod. Phys.* **83**, 543 (2011).
 - [3] T. Kampfrath, K. Tanaka, and K. A. Nelson, Resonant and non-resonant control over matter and light by intense terahertz transients, *Nat. Photon.* **7**, 680 (2013).
 - [4] T. Dong, S.-J. Zhang, and N.-L. Wang, Recent Development of Ultrafast Optical Characterizations for Quantum Materials, *Adv. Mater.* **35**, 2110068 (2023).
 - [5] J. Neu and C. A. Schmuttenmaer, Tutorial: An introduction to terahertz time domain spectroscopy (THz-TDS), *J. Appl. Phys.* **124**, 231101 (2018).
 - [6] D. N. Basov, R. D. Averitt, and D. Hsieh, Towards properties on demand in quantum materials, *Nat. Mater.* **16**, 1077 (2017).
 - [7] A. de la Torre, D. M. Kennes, M. Claassen, S. Gerber, J. W. McIver, and M. A. Sentef, Colloquium: Non-thermal pathways to ultrafast control in quantum materials, *Rev. Mod. Phys.* **93**, 041002 (2021).
 - [8] D. Fausti, R. I. Tobey, N. Dean, S. Kaiser, A. Dienst, M. C. Hoffmann, S. Pyon, T. Takayama, H. Takagi, and A. Cavalleri, Light-Induced Superconductivity in a Stripe-Ordered Cuprate, *Science* **331**, 189 (2011).
 - [9] E. Rowe, B. Yuan, M. Buzzi, G. Jotzu, Y. Zhu, M. Fechner, M. Först, B. Liu, D. Pontiroli, M. Riccò, and A. Cavalleri, Resonant enhancement of photo-induced superconductivity in K₃C₆₀, *Nat. Phys.* **19**, 1821 (2023).
 - [10] S. Fava, G. De Vecchi, G. Jotzu, M. Buzzi, T. Gebert, Y. Liu, B. Keimer, and A. Cavalleri, Magnetic field expulsion in optically driven YBa₂Cu₃O_{6.48}, *Nature* **632**, 75 (2024).
 - [11] S. Schlauderer, C. Lange, S. Baierl, T. Ebnet, C. P. Schmid, D. C. Valovcin, A. K. Zvezdin, A. V. Kimel, R. V. Mikhaylovskiy, and R. Huber, Temporal and spectral fingerprints of ultrafast all-coherent spin switching, *Nature* **569**, 383 (2019).
 - [12] Z. Zhang, M. Kanega, K. Maruyama, T. Kurihara, M. Nakajima, T. Tachizaki, M. Sato, Y. Kanemitsu, and H. Hirori, Spin switching in Sm_{0.7}Er_{0.3}FeO₃ triggered by terahertz magnetic-field pulses, *Nat. Mater.* **24**, 219 (2025).
 - [13] Y. Tokura, M. Kawasaki, and N. Nagaosa, Emergent functions of quantum materials, *Nat. Phys.* **13**, 1056 (2017).
 - [14] H.-K. Mao, X.-J. Chen, Y. Ding, B. Li, and L. Wang, Solids, liquids, and gases under high pressure, *Rev. Mod. Phys.* **90**, 015007 (2018).
 - [15] A. Yamamoto, N. Takeshita, C. Terakura, and Y. Tokura, High pressure effects revisited for the cuprate superconductor family with highest critical temperature, *Nat. Commun.* **6**, 8990 (2015).

- [16] A. Leitenstorfer, A. S. Moskalenko, T. Kampfrath, J. Kono, E. Castro-Camus, K. Peng, N. Qureshi, D. Turchinovich, K. Tanaka, A. G. Markelz, M. Havenith, C. Hough, H. J. Joyce, W. J. Padilla, B. Zhou, K.-Y. Kim, X.-C. Zhang, P. U. Jepsen, S. Dhillon, M. Vitiello, E. Linfield, A. G. Davies, M. C. Hoffmann, R. Lewis, M. Tonouchi, P. Klarskov, T. S. Seifert, Y. A. Gerasimenko, D. Mihailovic, R. Huber, J. L. Boland, O. Mitrofanov, P. Dean, B. N. Ellison, P. G. Huggard, S. P. Rea, C. Walker, D. T. Leisawitz, J. R. Gao, C. Li, Q. Chen, G. Valušis, V. P. Wallace, E. Pickwell-MacPherson, X. Shang, J. Hesler, N. Ridler, C. C. Renaud, I. Kallfass, T. Nagatsuma, J. A. Zeitler, D. Arnone, M. B. Johnston, and J. Cunningham, The 2023 terahertz science and technology roadmap, *J. Phys. D: Appl. Phys.* **56**, 223001 (2023).
- [17] X. B. Wang, H. Wang, J. Y. Yuan, X. Y. Zeng, L. Cheng, J. Qi, J. L. Luo, T. Dong, and N. L. Wang, Table-top laser-based terahertz high harmonic generation spectroscopy under magnetic fields and low temperatures, *Rev. Sci. Instrum.* **95**, 103007 (2024).
- [18] T. Dong, Z. G. Chen, and N. L. Wang, Magneto optics and time resolved terahertz spectroscopy, *Chin. Phys. B* **27**, 077501 (2018).
- [19] L. Duvillaret, F. Garet, and J. Coutaz, A reliable method for extraction of material parameters in terahertz time-domain spectroscopy, *IEEE J. Sel. Top. Quantum Electron.* **2**, 739 (1996).
- [20] F. Chen, X. Bai, Y. Wang, T. Dong, J. Shi, Y. Zhang, X. Sun, Z. Wei, M. Qin, J. Yuan, Q. Chen, X. Wang, X. Wang, B. Zhu, R. Huang, K. Jiang, W. Zhou, N. Wang, J. Hu, Y. Li, K. Jin, and Z. Zhao, Emergence of superconducting dome in ZrN_x films via variation of nitrogen concentration, *Sci. Bull.* **68**, 674 (2023).
- [21] L. Shi, X. Li, R. Li, Y. Li, T. Dong, J. Luo, X. Wang, and N. Wang, Field and temperature evolution of the magnetic excitations in the field-induced state of $Na_2Co_2TeO_6$, *Phys. Rev. B* **112**, 184406 (2025).
- [22] Q. Li, H. Shen, J. Luo, A. Wu, X. Wang, A. M. Kalashnikova, J. Xu, and L. Su, Anomalous magnetic field-dependent spin dynamics in $Gd_{0.3}Ho_{0.7}FeO_3$ single crystal near the ordering temperature of rare-earth ions, *Appl. Phys. Lett.* **128**, 082408 (2026).
- [23] Z. Fu, J. Chen, J. Shang, X. Lin, P. Suo, K. Sun, C. Wang, Q. Li, J. Luo, X. Wang, A. Wu, and G. Ma, Magnon and electromagnon excitations in $Dy_{0.9}Nd_{0.1}FeO_3$ single crystals tuned with temperature and magnetic field, *Appl. Phys. Lett.* **125**, 241102 (2024).
- [24] J. Chen, Q. Li, Z. Fu, J. Shang, P. Suo, X. Lin, J. Luo, X. Wang, A. Wu, and G. Ma, Terahertz cavity magnon-polaritons in $Gd_{0.5}Ho_{0.5}FeO_3$ single crystals tuned with temperature and magnetic field, *Appl. Phys. Lett.* **127**, 062402 (2025).
- [25] D. Nicoletti and A. Cavalleri, Nonlinear light-matter interaction at terahertz frequencies, *Adv. Opt. Photonics* **8**, 401 (2016).
- [26] P. Salén, M. Basini, S. Bonetti, J. Hebling, M. Krasilnikov, A. Y. Nikitin, G. Shamuilov, Z. Tibai, V. Zhaunerchyk, and V. Goryashko, Matter manipulation with extreme terahertz light: Progress in the enabling THz technology, *Phys. Rep.* **836-837**, 1 (2019).
- [27] C. Huang, M. Mootz, L. Luo, I. E. Perakis, and J. Wang, Terahertz 2D coherent spectroscopy for probing and controlling multicorrelations in quantum matter, *Nat. Rev. Phys.* **8**, 171 (2026).
- [28] J. Hebling, K.-L. Yeh, M. C. Hoffmann, B. Bartal, and K. A. Nelson, Generation of high-power terahertz pulses by tilted-pulse-front excitation and their application possibilities, *J. Opt. Soc. Am. B* **25**, B6 (2008).
- [29] X. B. Wang, L. Y. Shi, S. J. Zhang, J. Y. Yuan, Y. T. Li, J. L. Luo, T. Dong, and N. L. Wang, A versatile two-dimensional terahertz spectroscopy platform with dual independently controlled intense pulses, *Rev. Sci. Instrum.* **97**, 033001 (2026).
- [30] P. Peng, Z. L. Li, and X. B. Wang, Terahertz-field-induced second harmonic generation in weyl semimetal TaAs, *Chin. J. Lasers* **50**, 1714016 (2023).
- [31] S. Mansourzadeh, T. Vogel, A. Omar, T. O. Buchmann, E. J. R. Kelleher, P. U. Jepsen, and C. J. Saraceno, Towards intense ultra-broadband high repetition rate terahertz sources based on organic crystals [Invited], *Opt. Mater. Express* **13**, 3287 (2023).
- [32] M. Shalaby and C. P. Hauri, Demonstration of a low-frequency three-dimensional terahertz bullet with extreme brightness, *Nat. Commun.* **6**, 5976 (2015).
- [33] A. Sell, A. Leitenstorfer, and R. Huber, Phase-locked generation and field-resolved detection of widely tunable terahertz pulses with amplitudes exceeding 100 MV/cm, *Opt. Lett.* **33**, 2767 (2008).
- [34] B. Liu, H. Bromberger, A. Cartella, T. Gebert, M. Foerst, and A. Cavalleri, Generation of narrowband, high-intensity, carrier-envelope phase-stable pulses tunable between 4 and 18 THz, *Opt. Lett.* **42**, 129 (2017).
- [35] M. Reid and R. Fedosejevs, Quantitative comparison of terahertz emission from (100) InAs surfaces and a GaAs large-aperture photoconductive switch at high fluences, *Appl. Opt.* **44**, 149 (2005).
- [36] T. Lin, R. Xu, X. Chen, Y. Guan, M. Yao, J. Zhang, X. Li, and H. Zhu, Subwavelength, Phase-Sensitive Microscopy of Third-Order Nonlinearity in Terahertz Frequencies, *ACS Photonics* **11**, 33 (2023).
- [37] W. Li, S. Wang, P. Peng, H. Han, X. Wang, J. Ma, J. Luo, J.-M. Liu, J.-F. Li, C.-W. Nan, and Q. Li, Terahertz excitation of collective dynamics of polar skyrmions over a broad temperature range, *Nat. Phys.* **21**, 1965 (2025).
- [38] Y. Gao, X. Y. Zeng, X. B. Wang, Y. G. Shi, L. Cheng, and J. Qi, Terahertz manipulation of nonlinear optical response in topological material $PtBi_2$, *Opt. Lett.* **49**, 3862 (2024).
- [39] X. Li, T. Qiu, J. Zhang, E. Baldini, J. Lu, A. M. Rappe, and K. A. Nelson, Terahertz field-induced ferroelectricity in quantum paraelectric $SrTiO_3$, *Science* **364**, 1079 (2019).
- [40] W. Li, H. Kim, X. Wang, J. Luo, S. Latini, D. Shin, J.-M. Liu, J.-F. Li, A. Rubio, C.-W. Nan, and Q. Li, A Hidden Quantum Paraelectric Phase in $SrTiO_3$ Induced by Terahertz Field, *arXiv:2412.20887* (2024).
- [41] C.-J. Yang, J. Li, M. Fiebig, and S. Pal, Terahertz control of many-body dynamics in quantum materials, *Nat. Rev. Mater.* **8**, 518 (2023).
- [42] H. A. Hafez, S. Kovalev, J.-C. Deinert, Z. Mics, B. Green, N. Awari, M. Chen, S. Germanskiy, U. Lehnert, J. Teichert, Z. Wang, K.-J. Tielrooij, Z. Liu, Z. Chen, A. Narita, K. Müllen, M. Bonn, M. Gensch, and D. Turchinovich, Extremely efficient terahertz high-harmonic generation in graphene by hot Dirac fermions, *Nature* **561**, 507 (2018).
- [43] H. Chu, M.-J. Kim, K. Katsumi, S. Kovalev, R. D. Dawson, L. Schwarz, N. Yoshikawa, G. Kim, D. Putzky, Z. Li, H. Raffy, S. Germanskiy, J.-C. Deinert, N. Awari, I. Ilyakov, B. Green, M. Chen, M. Bawatna, G. Cristiani, G. Logvenov, Y. Gallais, A. V. Boris, B. Keimer, A. P. Schnyder, D. Manske, M. Gensch, Z. Wang, R. Shimano, and S. Kaiser, Phase-resolved Higgs response in superconducting cuprates, *Nat. Commun.* **11**, 1793 (2020).
- [44] H. Wang, J. Yuan, H. Shi, H. Li, X. Jia, X. Song, L. Shi, T. Wu, L. Yue, Y. Li, K. Jin, D. Wu, J. Luo, X. Wang, T. Dong, and

- N.-L. Wang, Anomalous terahertz nonlinearity in disordered *s*-wave superconductor close to the superconductor-insulator transition, *Phys. Rev. Lett.* **136**, 146004 (2026).
- [45] Y. Yang, Y. H. Meng, B. R. Lu, F. Jin, Y. G. Shi, F. Hong, S. S. Zhang, X. H. Yu, X. B. Wang, and J. L. Luo, Ultrafast carrier and phonon dynamics in Bi₂Se₃ under high pressure, *Phys. Rev. B* **109**, 064307 (2024).
- [46] Y. Meng, W. Mao, L. Chen, E. E. M. Chia, Y. Yang, J. Luo, L. Zhao, X. Zhou, X. Yu, and X. B. Wang, Ultrafast decoupling of the pseudogap from superconductivity in a pressurized cuprate, [arXiv:2604.10207](https://arxiv.org/abs/2604.10207) (2026).
- [47] Y. Meng, Y. Yang, H. Sun, S. Zhang, J. Luo, L. Chen, X. Ma, M. Wang, F. Hong, X. Wang, and X. Yu, Density-wave-like gap evolution in La₃Ni₂O₇ under high pressure revealed by ultrafast optical spectroscopy, *Nat. Commun.* **15**, 10408 (2024).
- [48] M. P. Fischer, J. Bühler, G. Fitzky, T. Kurihara, S. Eggert, A. Leitenstorfer, and D. Brida, Coherent field transients below 15 THz from phase-matched difference frequency generation in 4H-SiC, *Opt. Lett.* **42**, 2687 (2017).
- [49] C. Vicario, A. Trisorio, S. Allenspach, C. Rüegg, and F. Giorgianni, Narrow-band and tunable intense terahertz pulses for mode-selective coherent phonon excitation, *Appl. Phys. Lett.* **117**, 101101 (2020).
- [50] A. Cartella, T. F. Nova, A. Oriana, G. Cerullo, M. Först, C. Manzoni, and A. Cavalleri, Narrowband carrier-envelope phase stable mid-infrared pulses at wavelengths beyond 10 μ m by chirped-pulse difference frequency generation, *Opt. Lett.* **42**, 663 (2017).
- [51] M. Basini, M. Pancaldi, B. Wehinger, M. Udina, V. Unnikandanunni, T. Tadano, M. C. Hoffmann, A. V. Balatsky, and S. Bonetti, Terahertz electric-field-driven dynamical multiferroicity in SrTiO₃, *Nature* **628**, 534 (2024).
- [52] O. Minakova, C. Paiva, M. Frenzel, M. S. Spencer, J. M. Urban, C. Ringkamp, M. Wolf, G. Mussler, D. M. Juraschek, and S. F. Maehrlein, Observation of angular momentum transfer among crystal lattice modes, *Nat. Phys.* (2026).